molecular pharmaceutics

Article

pubs.acs.org/molecularpharmaceutics

Design, Synthesis and Biological Assessment of a Triazine Dendrimer with Approximately 16 Paclitaxel Groups and 8 PEG Groups

Changsuk Lee,[†] Su-Tang Lo,[‡] Jongdoo Lim,[†] Viviana C. P. da Costa,[†] Saleh Ramezani,[‡] Orhan K. Öz,[‡] Giovanni M. Pavan,[∥] Onofrio Annunziata,[†] Xiankai Sun,[‡,§] and Eric E. Simanek*,[†]

[†]Department of Chemistry, Texas Christian University, Fort Worth, Texas 76129, United States

[‡]Department of Radiology and [§]Advanced Imaging Research Center, University of Texas Southwestern Medical Center, Dallas, Texas 75390, United States

[∥]Laboratory for Innovative Technologies, University of Applied Science of Southern Switzerland, Galleria 2, 6829, Manno, Switzerland

Supporting Information

ABSTRACT: The synthesis and characterization of a generation three triazine dendrimer that displays a phenolic group at the core for labeling, up to eight 5 kDa PEG chains for solubility, and 16 paclitaxel groups is described. Three different diamine linkers—dipiperidine trismethylene, piperazine, and aminomethylpiperidine—were used within the dendrimer. To generate the desired stoichiometric ratio of 8 PEG chains to 16 paclitaxel groups, a monochlorotriazine was prepared with two paclitaxel groups attached through their 2′-hydroxyls using a linker containing a labile disulfide. This monochlorotriazine was linked to a dichlorotriazine with aminomethylpiperidine. The resulting dichlorotriazine bearing two paclitaxel groups could be reacted with the eight amines of the dendrimer. NMR and MALDI-TOF confirm successful reaction. The eight monochlorotriazines of the resulting material are used as the site for PEGylation affording the desired 2:1 stoichiometry. The target and intermediates were amenable to characterization by ^{1}H and ^{13}C NMR, and mass spectrometry. Analysis revealed that 16 paclitaxel groups were installed along with 5−8 PEG chains. The final construct is 63% PEG, 22% paclitaxel, and 15% triazine dendrimer. Consistent with previous efforts and computational models, 5 kDa PEG groups were essential for making the target water-soluble. Molecular dynamics simulations showed a high degree of hydration of the core, and a radius of gyration of 2.8 ± 0.2 nm. The hydrodynamic radius of the target was found to be 15.8 nm by dynamic light scattering, an observation indicative of aggregation. Drug release studies performed in plasma showed slow and identical release in mouse and rat plasma (8%, respectively). SPECT/CT imaging was used to follow biodistribution and tumor uptake. Using a two component model, the elimination and distribution half-lives were 2.65 h and 38.2 h, respectively. Compared with previous constructs, this dendrimer persists in the vasculature longer (17.33 ± 0.88% ID/g at 48 h postinjection), and showed higher tumor uptake. Low levels of dendrimer were observed in lung, liver, and spleen (~6% ID/g). Tumor saturation studies of small prostate cancer tumors (PC3) suggest that saturation occurs at a dose between 23.2 mg/kg and 70.9 mg/kg.

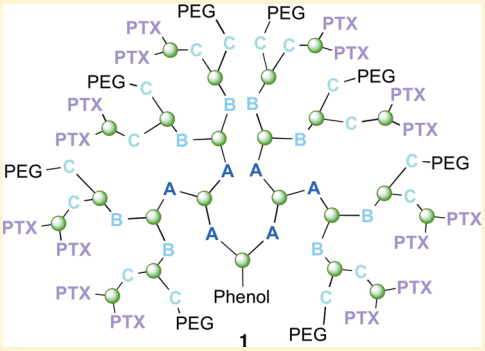

1

KEYWORDS: *paclitaxel, triazine, dendrimer, disulfide linkage, biodistribution, drug delivery, simulation, molecular dynamics*

INTRODUCTION

Paclitaxel has been extensively studied[1,2] because of its therapeutic efficacy against a wide range of cancers including those of the breast,[3−5] ovaries,[6] and prostate,[7] as well as AIDS related Kaposi's sarcoma.[8] In addition, its poor water solubility (<0.1 μg/mL) requires that paclitaxel be administered with a carrier. Originally, cosolvents such as Cremophor EL (polyoxyethylated castor oil) or polysorbate 80 formulations were adopted, although these can cause severe allergic reactions in some patients.[9−13] Abraxane, albumin bound paclitaxel, is an example of a successful nanoscale drug delivery formulation that has been approved by the FDA.[14,15] While overcoming the challenges of the original additives, Abraxane, like all chemotherapies, leads to undesirable toxicities and side affects due to the dose utilized and off-target affects.

Polymer-based drug delivery, described first by Ringsdorf[16] and bolstered by the advantages that the enhanced permeation and retention that tumors show toward large molecules,[17] has been broadly embraced by chemists pursuing a range of architectures. Macromolecular drug delivery agents such as polyplexes, polymeric micelles, dendritic core−shell architectures, or nanoparticle depots have continued to attract interest due to their low toxicities, their extended lifetimes within the circulatory system, and their ability to convey solubility to the

Received: May 17, 2013
Revised: September 10, 2013
Accepted: October 17, 2013
Published: October 17, 2013

Chart 1. Paclitaxel-Conjugated Triazine Dendrimers 1−3[a]

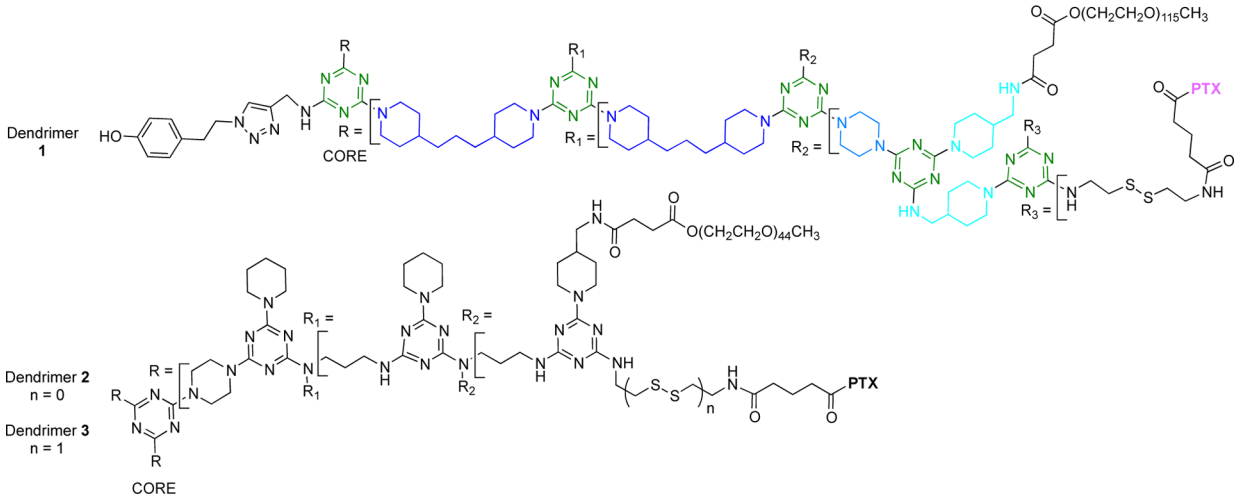

[a]Both **1** and **3** have disulfide linkers. Colors reflect those used in Scheme 1. PTX = paclitaxel.

drug cargo.[18] Dendrimers bearing paclitaxel have been the focus of our efforts and those of others.[19] Advantages of triazines include ease of synthesis; stability; structurally and compositionally well-defined, globular structure; opportunities for achieving acceptable drug loadings; and low polydispersity.[20−24]

The target described here, **1**, is the fourth in a series of agents that have been iteratively prepared and refined to address questions of chemistry and biological activity. Chart 1 shows **1** and two previously described prodrugs, **2** and **3**.[25−28] Prodrugs **2** and **3** present twelve paclitaxel groups and have sites for up to 12 PEG chains. The activity of **3** was markedly improved in vivo compared to that of **2** presumably due to the labile disulfide.[29−31] Dosing mice with **3** at 50 mg/kg weekly over three weeks led to tumor reduction/disappearance without mortality.[25] However, installation of twelve 2 kDa PEG chains was problematic. The result of the synthesis was a mixture of dendrimers displaying between 6 and 12 chains. Here, we aimed to reduce heterogeneity by reducing the number of PEGylation reactions that are performed, while simultaneously increasing the number of paclitaxel groups on the dendrimer.

EXPERIMENTAL SECTION

Synthesis. The experimental details for synthesis including spectra can be found in the Supporting Information.

HPLC Based Assessments of Purity. The chromatographic system used to measure sample purity consisted of a degasser (Agilent G1379B, Palo Alto, CA), capillary pump (Agilent G1312B), micro well-plate auto sampler (Agilent G1367D), Zorbax 300SB-C8 column (1.0 mm i.d. × 150 mm, 3.5 μm, Agilent), and a diode array detector (Agilent G1316B). The mobile phase consisted of water/acetonitrile (A/B, HPLC grade, 0.1% (w/v) trifluoroacetic acid) at a flow rate of 50 μm/min. The elution gradient was 35% MeCN for 5 min, ramp to 80% MeCN in 20 min, hold at 80% MeCN for 10 min, and ramp down to 35% MeCN in 10 min. The sample volume injected 5 μL at a concentration of 0.64 mg/mL in HPLC-grade MeCN. The sample was detected at 227 nm. Samples were run in triplicate.

Paclitaxel Release of Dendrimer 1 in Plasma. To determine the rate of release of bound paclitaxel from **1** in plasma, a solution of **1** (500 μL, 300 μg/mL in PBS buffer) was incubated in 100 μL of plasma (rat or mouse) at 37 °C for 48 h. At selected time intervals (0.5, 1, 6, 24, and 48 h), the plasma samples were mixed with 500 μL of ice-cold acetonitrile that contained 10 μL of 366 μg/mL docetaxel as an internal standard. The samples were then centrifuged at 14000 rpm for 20 min to remove precipitated protein, and 10 μL of aliquots were injected into an HPLC system. HPLC analysis was performed using the same Agilent system, column, and elution gradient. The internal standard, docetaxel, and analyte, paclitaxel, elution times were 14−16 and 17−19 min, respectively. The peak area ratio was used to calculate paclitaxel concentrations.

Paclitaxel Release of Model Compound 12 in Plasma. In order to determine the rate of release of bound paclitaxel from the model compound **12** in plasma, a solution of model compound **12** (50 μL, *c* 1.0 mg/mL in DMSO) was incubated in 500 μL of PBS buffer and 100 μL of plasma (rat or mouse) at 37 °C for 20 h. At selected time intervals (6 and 20 h), the plasma samples were mixed with 500 μL of ice-cold acetonitrile that contained 20 μL of 392 μg/mL docetaxel as an internal standard. The samples were then centrifuged at 14000 rpm for 20 min to remove precipitated protein, and 5 μL of aliquots were injected into an HPLC system. HPLC analysis was performed using the same Agilent system, column, and elution gradient. The elution times for the compounds were as follows: docetaxel (15−17 min), paclitaxel (18−19 min), and model compound **12** (14−16 min). The peak area ratio was used to calculate paclitaxel concentrations.

Methods in Molecular Dynamics Simulation. The experimental procedure followed published methods.[25,32] Briefly, the molecular models were built from different residues according to previous studies on similar dendrimers.[33] All of the nonstandard residues were obtained according to a well-validated procedure adopted by our group.[34] All molecular dynamics simulations (MD) were conducted using the AMBER 11 suite of programs.[35] The dendrimers were solvated in a periodic box with a 14 Å buffer containing explicit TIP3P[36] water molecules and a suitable number of Cl^- and Na^+ ions necessary to guarantee overall neutrality and to reproduce the experimental salt concentration of 150 mM NaCl. The single 5 kDa linear PEG chains were preliminarily prefolded in vacuum to reduce the initial size of the simulation box and, accordingly, the number of water molecules necessary for solvation. This procedure is consistent with previously reported simulation studies of molecular systems containing long PEG chains,[37] and

dx.doi.org/10.1021/mp400290u | *Mol. Pharmaceutics* 2013, 10, 4452−4461

with the well-demonstrated tendency of PEG to fold in solution.[33] The dendrimers were first minimized and then equilibrated for 50 ns in NPT condition at the temperature of 300 K and pressure of 1 atm. During this time all molecular systems reached equilibrium with good stability. Simulations were conducted using a time step of 2 fs, a Langevin thermostat, a 10 Å cutoff, the particle mesh Ewald[38] (PME) approach to treat long-range electrostatic interactions, and the SHAKE algorithm.[39] The *parm99* all-atom force field by Cornell et al.[40] was used for all of the standard residues present in the systems. The radius of gyration (R_g) and the radial distribution functions (RDFs) of the dendrimers were calculated by processing the equilibrated dynamic trajectories with the *ptraj* module of AMBER 11.

Dynamic Light Scattering. Samples were prepared by weight starting from stock solutions with concentrations of the order of 10 g/L (1% w/w). DLS measurements were performed in the range 0.3−5 g/L in PBS at 25 °C and at the angle of 90°. Samples were filtered through a 0.02 μm filter. The diffusion coefficient was measured as a function of concentration and extrapolated to zero concentration to determine the hydrodynamic radius of the **1**.

Radiolabeling of Prodrug 1 with ^{125}I. IODO-GEN precoated iodination tubes (Pierce, Rockford, IL) were used for labeling of **1** with ^{125}I at the Bolton−Hunter moiety. In brief, the IODO-GEN precoated tubes were rinsed with 1 mL of 10 mM PBS buffer (pH 7.5) before the labeling. To each IODO-GEN tube containing 4.5 nmol of prodrug **1** in 20 mM PBS was added 1 mCi of Na^{125}I (2 μL). The solution was kept at room temperature for 20 min with gentle swirling every 5 min. The radiochemical reaction was monitored by iTLC. The sample was further purified by using Millipore centrifugal filtration unit (MWCO: 10K), which were centrifuged at 6,000 rpm for 60 min to remove the free ^{125}I ion or other small molecular species. The product was then washed with 3 portions of 1 mL of 10 mM PBS. Radio-TLC or radio-HPLC was used to measure the radiolabeling efficiency and determine the radiochemical purity of ^{125}I-labeled **1** (^{125}I-**1**).

Size Exclusion HPLC Assessment of the Association between 1 and Serum Proteins. ^{125}I-**1** was incubated with rat serum at 37 °C for 3 and 18 h. The serum samples of ^{125}I-**1** were analyzed by size-exclusion chromatography on a BioSuite 450 column (Waters; MW range: 20 kDa to 7000 kDa) at 1 mL/min (isocratic condition, mobile phase: 10 mM PBS, pH 7.0). The fractions were collected and then counted by a γ-counter (Perkin-Elmer). The serum samples of Na^{125}I were prepared side by side and used as controls in this assessment.

Biodistribution Study in Normal BALB/c Mice and PC-3 Tumor-Bearing Mice. To determine the in vivo tissue distribution of ^{125}I-**1**, the biodistribution study was first performed in normal BALB/c mice and then on PC-3 tumor bearing SCID mice. The prostate cancer mouse model was established by injecting PC-3 cells subcutaneously into both front flanks (2×10^6 of cells in 100 μL) of male SCID mice at 6−8 weeks of age. Tumors were allowed to grow for 3 weeks to reach the size of 10−100 mm^3. In the biodistribution study in normal mice, each mouse was intravenously injected with 100 μL of ^{125}I-**1** (10−15 μCi/mouse). Mice were sacrificed at 1, 4, 24, and 48 h postinjection (p.i.; $n = 4$). Harvested organs included blood, heart, lung, fat, liver, spleen, kidneys, stomach, muscle, femur, thyroid, brain, and thymus. For the biodistribution study in SCID mice bearing PC3 tumor, a similar dose of ^{125}I-**1** was injected and mice were sacrificed 48 h p.i. Tumor was excised from the PC-3 tumor-bearing mice. The tissue samples were weighed, and then their radioactivity was quantified by a γ-counter. Standards were prepared, weighed, and counted along with the samples for the calculation of percentage of injected dose per gram of tissue (% ID/g). Statistical analysis was performed using Prism 5.0 (Graphpad, San Diego, CA).

Tumor Saturation Dose Evaluation of ^{125}I-1 in PC-3 Tumor-Bearing Mice by Small Animal SPECT/CT Imaging. In the PC3 xenograft model, tumor necrosis is often observed when the tumor size is above 300 mm^3. To minimize this factor, the tumor size was controlled below 100 mm^3 in this imaging evaluation, which was performed on a small-animal NanoSPECT/CT PLUS system (Bioscan, Washington, DC, USA). Four paclitaxel equivalent dose groups of ^{125}I-**1** were used: 1.7, 23.2, 70.9, and 111.3 mg/kg ($n = 4$). The lowest dose (1.7 mg/kg) was the amount of purified ^{125}I-**1** injected directly into the tumor bearing mice for the imaging evaluation; the remaining doses were prepared by constituting the same amount of ^{125}I-**1** with cold prodrug **1**. In other words, the lowest dose (1.7 mg/kg) of prodrug **1** was used as the imaging tracer to evaluate the tumor saturation dose of ^{125}I-**1**. For each mouse, the injected radioactivity (^{125}I-**1**) was controlled within 300−500 μCi in 250 μL for SPECT/CT imaging. The injection dose was prepared by combining ^{125}I-**1** in 10 mM PBS with a concentrated cold prodrug **1** solution, which was made by dissolving the prodrug in 20% DMSO in 10 mM PBS with 30 min of sonication. After the intravenous injection of each dose, SPECT and CT images were acquired at 48 h p.i. The field of view (FOV) of the SPECT/CT was aimed at the shoulders of the mouse. The CT imaging was performed by 180 projections per rotation with 45 kVp, 1000 ms of exposure time, and the binning factor of 1:1. The SPECT imaging data were collected with 4 detector arrays collimated with multi-pinhole apertures giving a post-reconstruction resolution of 0.73 mm. The SPECT image reconstruction was carried out using HiSPECT NG with 35% smoothing, 100% resolution, and 9 iterations (Standard mode). The CT data were reconstructed using the Nucline v1.01 and a voxel size of 73 × 73 × 146 mm. Both SPECT and CT images were analyzed using the InVivoScope 2.00 software (Bioscan). Tumors smaller than 100 mm^3 were selected for imaging quantification. The volume of the region of interest (ROI) was based on the ex vivo size measurement. The standardized uptake value (SUV) was used for the SPECT/CT imaging quantification.

RESULTS AND DISCUSSION

Design. The design of target **1** was driven by three desires. First, a versatile handle for the incorporation of imaging agents was desired. Previous efforts with **2** and **3** relied on statistical, substoichiometric labeling of unreacted amine groups on the periphery of the dendrimer with a Bolton−Hunter agent. Instead, we incorporated an alkyne at the core that could be elaborated through click chemistry to yield the desired phenolic group, or other groups in the future. Second, improved synthetic efficiency was sought. Predecessors **2** and **3** derived from a generation two dendrimer whose synthesis included (i) extra capping steps as well as (ii) less reactive bis(3-aminopropyl)amine groups. Removing this capping step and improving the nucleophilicity of the surface amines were both goals of this effort. Incorporating trimethylene-dipiperidine and piperazine groups accomplished these goals. To reduce the number of PEG chains incorporated, fewer sites for PEGylation were incorporated into **1**. Based on the symmetry of the core, 16 paclitaxel and 8 PEG chains can be installed theoretically. By weight, **1** is 63% PEG, 22% paclitaxel, and 15% triazine dendrimer.

Scheme 1. Retrosynthetic Analysis[a]

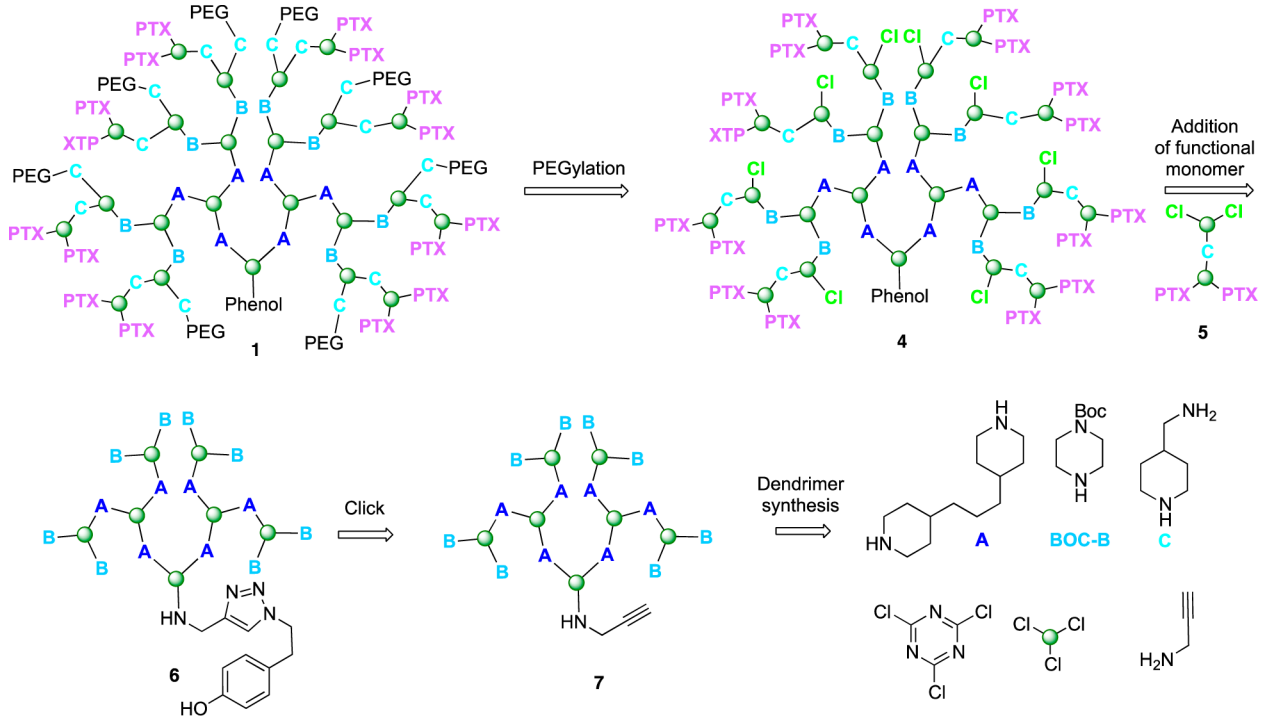

[a]Target **1** derives from a two-step PEGylation procedure of **4**. Intermediate **4** results from reaction of the functionalized dichlorotriazine bearing two paclitaxel groups (PTX), **5**, with dendrimer **6**. Dendrimer **6** comes from click reaction of **7**, which derives from some of the building blocks identified.

Scheme 2. Synthesis of the Generation Two Dendrimer

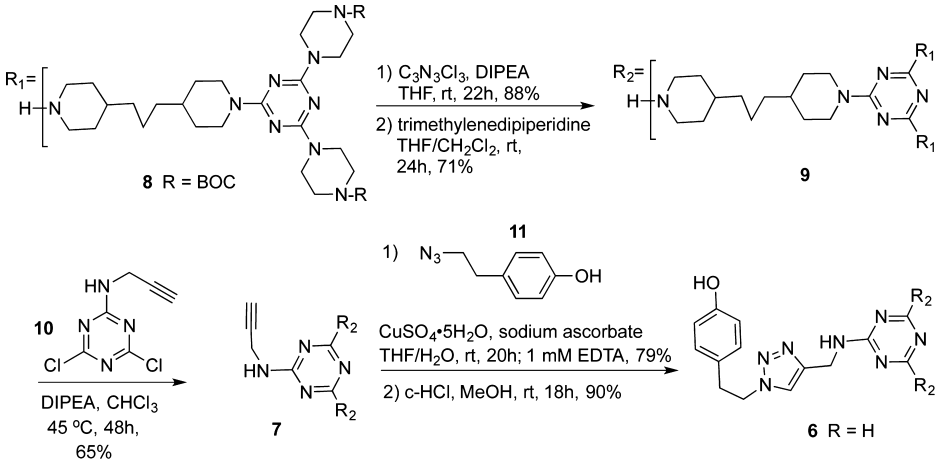

Synthesis. The synthesis of **1** proceeds in three phases: synthesis of the dendrimer, synthesis of the functional dichlorotriazine, and coupling the subunits with elaboration to the final product. The retrosynthetic analysis (Scheme 1) provides a schematic representation of the products and key intermediates. A key element is the two-step PEGylation procedure to yield **1**. This sequence relies on reacting poly(monochlorotriazine) **4** with aminomethylpiperidine followed by a commercially available PEG-NHS ester with a molecular weight of 5 kDa. To arrive at **4**, a dichlorotriazine monomer bearing two paclitaxel groups, **5**, is reacted with the generation two dendrimer **6**. Installation of the phenol for labeling relied on a click reaction at the core of dendrimer **7**. The building blocks utilized extensively throughout the synthesis are shown.

Dendrimer Synthesis. Scheme 2 shows the synthesis of **6**, the generation two dendrimer. Intermediate **8** can be rapidly obtained by reacting two equivalents of BOC-piperazine (BOC-B in Scheme 1) with cyanuric chloride followed by bispiperidine trismethylene (**A** in Scheme 1).[41] Continuing convergently, the process is iterated to obtain a generation two dendron, **9**. The core is installed with the alkyne-functionalized dichlorotriazine **10**. Click reaction[42,43] with **11** introduces a phenolic group[44] that can be subjected to radioiodination later. Overall, this six step procedure can be executed at 25% overall yield. Intermediates are purified by conventional silica gel chromatography, and provide satisfactory ^{1}H and ^{13}C NMR spectra and corroborating mass spectra.

dx.doi.org/10.1021/mp400290u | *Mol. Pharmaceutics* 2013, 10, 4452−4461

Scheme 3. Synthesis of the Dichlorotriazine

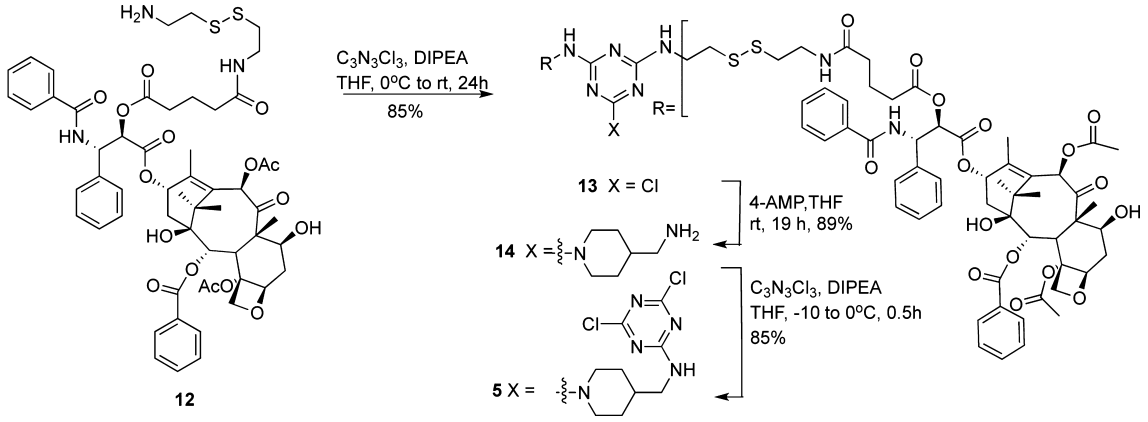

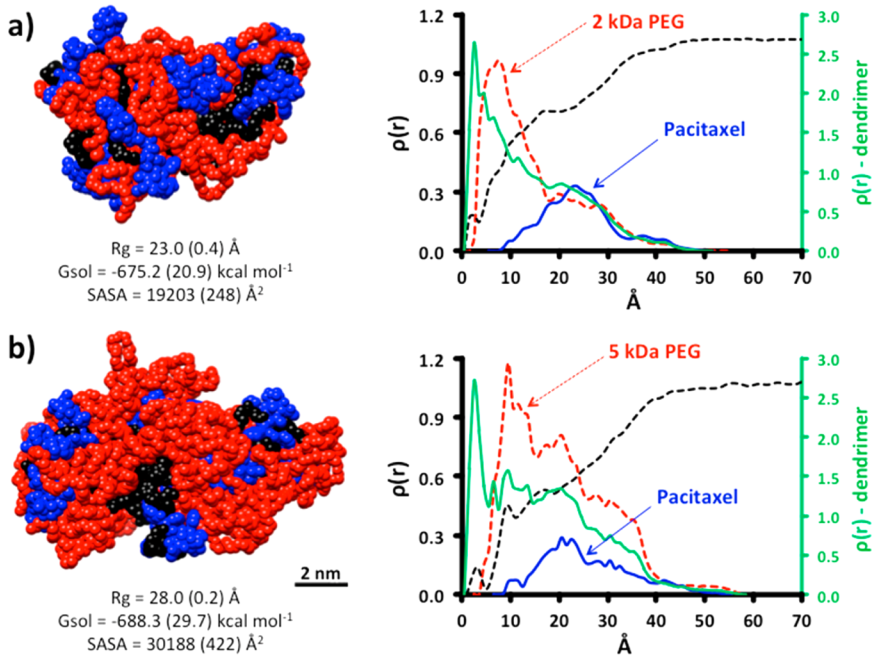

Figure 1. MD simulations show differences in size and solvent accessible surface area (SASA) for **4** PEGylated with 2 kDa PEG and 5 kDa PEG (**1**). Radial distribution functions show that 2 kDa PEG is insufficient in masking the hydrophobic dendrimer.

Synthesis of the Dichlorotriazine Bearing Paclitaxel. To arrive at the desired 2:1 stoichiometry of PTX:PEG, dichlorotriazine **5** was prepared (Scheme 3). Paclitaxel derivative **12** is available by reaction of paclitaxel with glutaric anhydride followed by formation of an NHS-ester with *N*-succinimidyl diphenylphosphate (SDPP), and then coupling with cysteamine.[26] The yield for this three step procedure was 67%. Reaction of **12** with cyanuric chloride provides **13**. This monochlorotriazine intermediate **13** was reacted with aminomethylpiperidine in 89% yield to provide **14**. Reaction of **14** with cyanuric chloride yields the reactive dichlorotriazine **5**. The overall yield for this six step sequence is 43%.

Elaboration by Coupling the Dichlorotriazine and Dendrimer Followed by PEGylation. Equation 1 shows the coupling of dendrimer **6** with dichlorotriazine **5**. Mass spectrometry can be used to monitor progress of the required 8 coupling reactions. The remaining 8 monochlorotriazine groups that appear on **4** are reacted first with aminomethylpiperidine, and then a commercially available 5 kDa PEG-NHS ester to yield **1**.[26,27] The solubility of **1** in water allowed for its purification from excess PEG by dialysis. Overall, the desired target is reached in 9 linear steps at 30% overall yield.

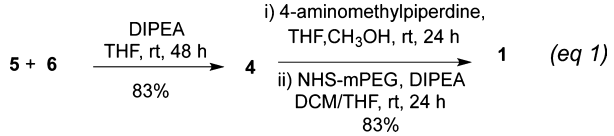

(eq 1)

Computation. Computational models provided insights into the impact of PEGylation on both solubility and drug shielding. The choice of 5 kDa PEG derived from intuition, experiment, and prediction. Intuitively, we believed 5 kDa PEG would be necessary because, with previous constructs, we found that a minimum of 2 kDa of PEG was required for each paclitaxel group. This belief was confirmed experimentally. We found that 2 kDa PEG groups were not sufficient to provide solublity in water, while using 5 kDa PEG did so.

MD simulations yield structures wherein PEG chains collapse around the surface of the dendimer, as seen in previous reports.[33,37] Simulation predicted that the hydrophobic surface

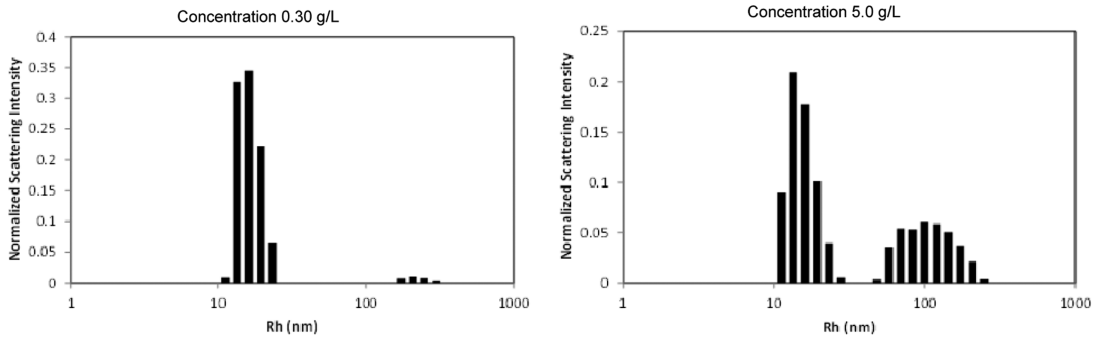

Figure 2. The light-scattering distribution analysis of prodrug **1**.

produced when **4** is reacted with 2 kDa PEG is significantly greater than when it is reacted with 5 kDa PEG (Figure 1). While the free energies of solvation calculated for both constructs were identical within standard deviation, the solvent exposed surface area was 1.6× greater when 5 kDa PEG was used. The radial distribution functions calculated from the equilibrated structures corroborate visual inspection of the minimized structures: the exposure of hydrophobic paclitaxel groups for the 2 kDa is greater than that of the 5 kDa structure. The green traces (plotted on a different scale) represent all the RDFs for all atoms in the construct. Colored traces shown in red and blue show the RDFs for PEG and paclitaxel groups, respectively, as colored in the molecular models appearing on the left. Water penetration, shown as a black dotted line, is similar in both constructs. Simulations support the expectation that paclitaxel groups are somewhat solvent accessible in **1**, but not to the degree that paclitaxel groups have been in previous triazine dendrimer prodrugs decorated with 2 kDa PEG chains.

Characterization. Throughout the synthesis, ^{1}H and ^{13}C spectroscopy and mass spectrometry provided compelling evidence of structure. Challenges to characterization arise during the final stages of any dendrimer synthesis. Evidence for successful reaction of the generation two dendrimer **6** with eight dichlorotriazines, **5**, can be observed by both the ^{1}H NMR spectroscopy and mass spectrometry. Integration of signals of the two protons of the phenolic group of the dendrimer and the ortho-protons of the two benzoyl groups of each of the 16 paclitaxel groups provides one estimate of the extent of reaction. The desired ratio of 2:32 is observed. This result is consistent with the spectrum obtained by MALDI-TOF mass spectrometry. The major species observed is the desired material showing a reasonable agreement between the calculated exact mass 22.7 kDa and the observed mass 22.8 kDa. Evidence for a minor species corresponding to 7 of the required 8 additions is also present. Two other species can be identified. The first represents loss of a single paclitaxel group at the 2′-ester. The second corresponds to cleavage at the disulfide. The extent to which these fragments represent impurities or arise during the ionization process is uncertain, but their value in anchoring assignment of the parent peak is invaluable.

PEGylation exacerbates the challenge of characterization. The ^{1}H NMR spectrum broadens further, but the ratio of 16 molecules of paclitaxel:dendrimer is maintained. Consistent with previous dendrimers bearing PEG, the mass spectrum derived from MALDI-MS shows a broad and largely featureless lump, here between 54 kDa and 68 kDa. The commercially available 5 kDa PEG reagent shows a distribution of masses from 5250 to 6250 centered at 5750. Because **4** has a mass of 22.8 kDa, PEGylation with 5 kDa PEG chains should yield a mass of ∼57 kDa upon installation of 6 PEG chains, and 68 kDa upon installation of 8 groups. Consistent with previous efforts, we conclude that PEGylation results in a mixture of products primarily comprising dendrimers with 5−8 PEG chains.

Confirming Distributions with HPLC. Reverse phase HPLC of **1** yields a chromatogram that is consistent with a mixture of PEGylated products with three major species identified. The chromatogram also shows that dialysis successfully removes free PEG.

Dynamic Light Scattering Supports Aggregation. Bovine serum albumin, which has a similar molecular weight as **1**, has a hydrodynamic radius of 3.5 nm. Computational models of monomeric **1** suggest similar protein-sized dimensions. However, dynamic light scattering (DLS) of **1** following filtration through a 20 nm filter reveals species with two different dimensions. The data was collected under conditions intended to reflect physiological conditions. The smaller of the two shows a hydrodynamic radius of **1** is 15.8 nm (Figure 2). The larger of the two exceeds 100 nm. The disparity is unlikely to be caused by swelling of the flexible PEG chains.[33] Instead, the difference in sizes is likely the result of the formation of aggregates in solution. Moreover, a concentration-dependent population of these two species is clearly visible when comparing solutions of 0.30 g/L and 5 g/L. As these histograms report normalized scattering intensity, the population of the larger species is likely to be 100−1000× exaggerated. A cloudy suspension is observed in bulk samples at concentrations of 10 g/L. No time dependent evolution of species was observed over 60 h. Molecular dynamics (MD) provides additional clues to structure.

Paclitaxel Release. Paclitaxel release was measured in mouse and rat plasma using an HPLC assay with docetaxel serving as an internal standard. While previous ester constructs showed release rates that differed with the source of plasma (8% in 24 h for mice; 20% in 24 h for rats), surprisingly no difference in release rates were observed for **1**: Both mouse and rat plasma showed 8% release at 24 h based on the amount of free paclitaxel observed. This nominal release may correspond to effective shielding of the drug by the larger PEG in models of a monomeric species or reflect a different behavior of aggregates of **1**, presumed to be the relevant species in solution. Indeed, the RDF plots derived from MD simulations suggest that PEG groups of **1** shield paclitaxel. However, simulations also reveal that both **1** and **3** should be porous with a high degree of solvent penetration with accessible disulfide and ester linkages.

To pursue this further, we prepared a model, **12**, and the expected cleavage products, **15** and **16**, to use as HPLC standards (Chart 2). All showed unique retention times by HPLC: **1** (40−42 min); **12** (13.7 min); **15** (31.5 min); **16** (28.4 min); paclitaxel (18 min); docetaxel (15 min).

Disulfides of 1 Are Cleaved with Reducing Agent. To establish that disulfide cleavage was possible, **1** was reduced

dx.doi.org/10.1021/mp400290u | *Mol. Pharmaceutics* 2013, 10, 4452−4461

Chart 2. Additional HPLC Standards with Sites of Cleavage of 1 Indicated with Arrows

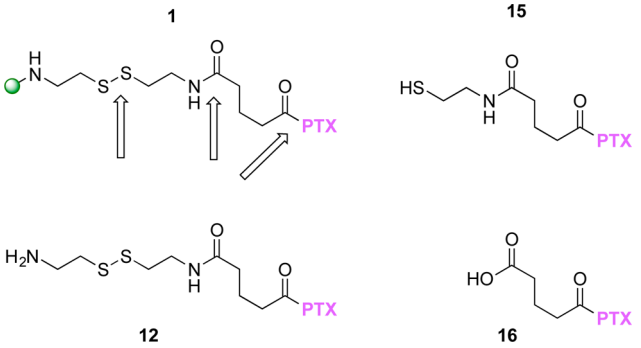

with dithiothreitol (DTT). By HPLC, two distinct features were observed. The first feature was a peak corresponding to the expected thiol, **15**. The second feature was a broad peak at 39 min that we attribute to the dendrimer after reduction based on the disappearance of a peak corresponding to **1**.

*Model **12** Is Reduced More Rapidly than **1**, but Differences between Mouse and Rat Plasma Are Observed.* After 20 h incubation in plasma, the amount of **12** was markedly reduced compared with **1**. There were no apparent differences in the rate of reduction of **12** between rat and mouse plasma. The peaks corresponding to **15** and **16** are obscured by signals derived from plasma, however. Paclitaxel was observed in the traces of rat plasma, but not in the traces obtained from mouse plasma. We conclude that the rate of ester hydrolysis varies with the source of plasma.

Biodistribution Studies. The radiosynthesis of ^{125}I-**1** provided a radiochemical yield of approximately 80% when the reaction ratio of ^{125}I versus prodrug **1** was maintained at 4 μCi/μg. After the separation by centrifugal filtration, the radiochemical purity of ^{125}I-**1** was nearly 100% as determined by radio-HPLC. The tissue distribution data are shown in Figure 3A. Because **1** showed high uptake and long retention in the blood, the scale of the *y*-axis was enlarged to better exhibit the tissue distribution profile of prodrug ^{125}I-**1** in other organs. Low uptake and accumulation were observed in the liver and spleen, while a relatively high uptake was observed in the lungs at 1 and 4 h p.i. The pharmacokinetic parameters (Figure 3B) were determined by a two-compartment model using the uptake levels of ^{125}I-**1** in the blood immediately after the injection to the end point of the biodistribution study. Dendrimer ^{125}I-**1** showed longer distribution and elimination half-lives ($t_{1/2\alpha}$ = 2.65 h; $t_{1/2\beta}$ = 38.2 h) than the dendrimer prodrugs that we previously published. For example, **3** with 12 paclitaxel and up to 12 PEG chains cleared much more rapidly with elimination and distribution half-lives of 0.4 h and 19.3 h ± 2.1 h, respectively. Dendrimer **1** was excreted mainly through urine (Figure 3C). However, due to the high retention in the blood, the excretion level was low. Taken in light of other efforts, including distribution parameters of different classes of dendrimers,[27] we hypothesize that **1** is aggregating in solution to form species that are too large for rapid renal clearance, yet successful at avoiding hepatic clearance and uptake by elements of the RES.

Tumor Saturation Dose Evaluation of ^{125}I-1 in PC-3 Tumor-Bearing Mice. Tumor saturation studies were performed to identify an optimal dose for further tumor treatment studies. By using the tracer concept, 4 different dosing groups were noninvasively assessed by SPECT/CT imaging with ^{125}I-**1**. Standardized uptake values (SUV) were used to quantitatively analyze the imaging results (Figure 4A). We find that as the tumors grew big, the tumor uptake values of ^{125}I-**1** scattered over a wide range, which likely resulted from the fact that the tumors become more heterogeneous at the same time. To minimize the variation caused by this tumor heterogeneity, the tumor size was controlled within 100 mm^3 and our quantitative imaging analysis was performed on tumors smaller than 40 mm^3 (Figures 4B and 4C). Shown in Figure 4A, tumors are clearly visualized by all dosing groups, in which the amount of injected radioactivity (^{125}I-**1**) was the same. Dilution of this dose with unlabeled **1** produced marked differences in uptake. Interestingly, the tumor uptake of ^{125}I-**1** (tracer) stayed at the same level when the injected dose was increased to 23.2 mg/kg dose (Figure 4A and 4C). This indicates that, in the dosing range of 1.7 mg/kg to 23.2 mg/kg, the tissue distribution profile of ^{125}I-**1** was the same. As the dose increased to 70.9 mg/kg, the tumor uptake was significantly reduced, indicating a dilution effect. From 70.9 mg/kg to 111.3 mg/kg, the dose of paclitaxel was increased by 1.57 times. Consistent mathematically, though rarely observed

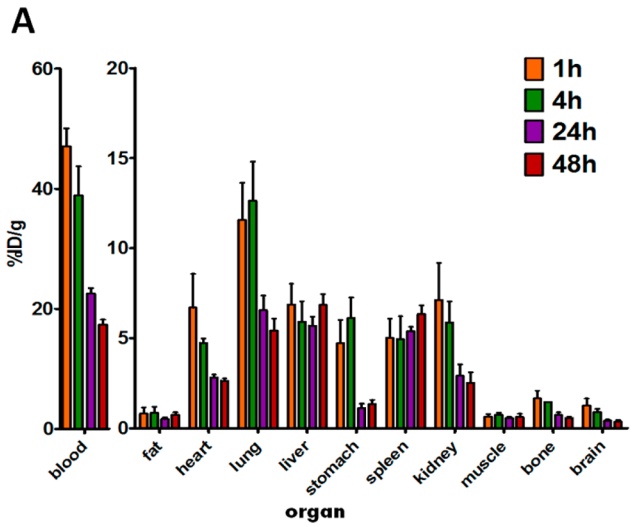

B

Pharmacokinetics (h)	
$t_{1/2\alpha}$	2.65
$t_{1/2\beta}$	38.23

C

Excretion Profiling (%ID)		
	Urine	Feces
24 h	4.25	0.27
48 h	5.47	0.36

Figure 3. (A) Tissue distribution of prodrug **1** in normal BALB/c mice. Data are presented as % ID/g ± SD (n = 4). (B) Pharmacokinetic parameters of prodrug **1** in normal BALB/c mice. (C) Excretion profile of prodrug **1** from BALB/c mice (n = 4).

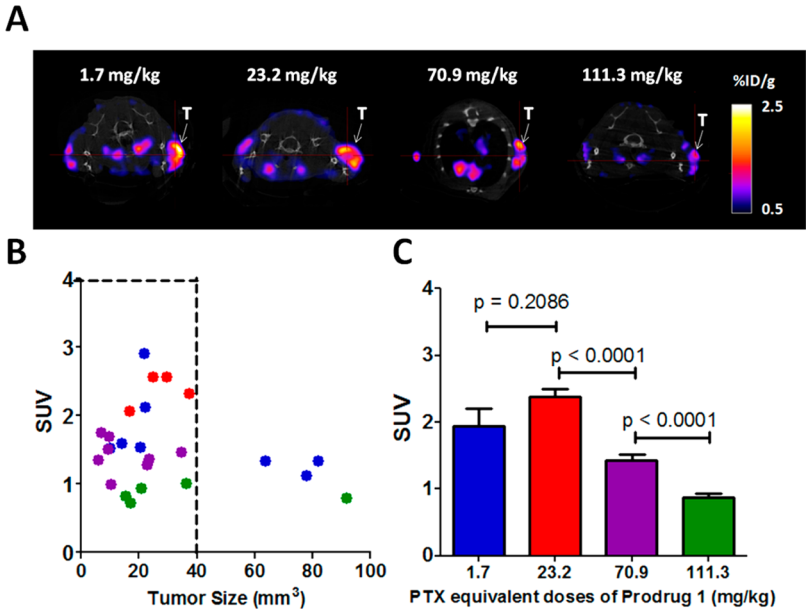

Figure 4. Tumor saturation dose evaluation of ^{125}I-**1** in PC-3 tumor-bearing mice: 1.7 mg/kg (blue), 23.2 mg/kg (red), 70.9 mg/kg (purple), and 111.3 mg/kg (green). (A) Representative transaxial SPECT/CT images of PC3 tumor in SCID mice (48 h p.i.). Tumors are indicated by white arrows. (B) Tumor uptake of ^{125}I-**1** versus tumor size. Tumors smaller than 100 mm^3 were selected for the evaluation. (Number of tumors evaluated in each group: 7 (1.7 mg/kg); 5 (23.2 mg/kg); 8 (70.9 mg/kg); 5 (111.3 mg/kg)). (C) Tumor uptake levels of the 4 dosing groups in tumors smaller than 40 mm^3. (Number of tumors evaluated in each group: 4 (1.7 mg/kg); 5 (23.2 mg/kg); 8 (70.9 mg/kg); 4 (111.3 mg/kg)). SUV is standardized uptake value of the labeled prodrug.

experimentally, the tumor uptake decreased by a similar extent (1.64), corresponding to the diluting factor of the tracer (^{125}I-**1**). The theoretical match between dilution and tumor uptake also suggests that prodrug **1** behaves similarly in vivo across the dosing range of the studies: dose-dependent precipitation or aggregation should significantly impact the saturation study. These observations lead us to conclude that the tumor saturation dose of prodrug **1** occurs between 23.2 mg/kg and 70.9. Mathematically extrapolated, an estimate of 50 mg/kg is obtained, a value consistent with dosings of previous prodrugs.

CONCLUSION

In summary, we have described the preparation of a dendrimer with a 2:1 ratio of paclitaxel:PEG chains with a site for a single label. Both NMR and mass spectrometry of **1** show that the paclitaxel groups undergo little to no hydrolysis during the final steps of the synthesis including purification by dialysis. The target contains 16 paclitaxel (22 wt % drug) and five to eight PEG arms (63 wt % PEG) with dendrimer comprising the smallest portion (15%). A minor contributor to the mixture is a dendrimer with 14 paclitaxels and 6 or 7 PEG chains. While simulations reveal that water penetration and accessibility in **1** were better than in previous constructs, the amount of released paclitaxel was lower in plasma in comparison. Model drug release studies in mouse plasma suggest the reduction of disulfide bond is much faster than hydrolysis of the ester. Three lines of evidence are consistent with aggregation of **1** into larger, discrete nanoparticles. First, dynamic light scattering reveals a dimension of 15.8 nm, which is significantly larger than the value obtained from computation, 2.3 nm. Second, ^{125}I-**1** shows significant concentrations in the vasculature over time and slow clearance. Third, this behavior is consistent with previously studied PEGylated triazine dendrimers bearing paclitaxel. Tumor saturation studies suggest that for small tumors, those not exceeding 40 mm^3, saturation occurs at doses less than 70.9 mg/kg. This range is consistent with doses ordinarily used for Taxol and Abraxane formulations of paclitaxel in mouse models as well as efficacious doses seen in previous triazine dendrimer prodrugs. These previous prodrugs showed similar drug release rates as **1**. The lack of a clear therapeutic advantage based on these release rates and tumor saturation data dissuades us from tumor regression studies at this point. Indeed, once tumor saturation is reached, the remainder of the injected dose should not impact the therapeutic efficacy, but rather be excreted or accumulate in nontarget organs causing unwanted side effects. Hypothetically, any benefit derived from **1** over clinically relevant formulations Taxol and Abraxane in this model of disease falls to the presence of a labeling group for theranostic applications, and/or the potential opportunity to reduce dosing frequency due to the long vasculature half-life.

ASSOCIATED CONTENT

Supporting Information

Additional experimenal details including synthetic prodecures, mass and NMR spectra, HPLC traces, light-scattering distribution analysis, cumulative PTX release graph, and cumulative excretion data. This material is available free of charge via the Internet at http://pubs.acs.org.

AUTHOR INFORMATION

Corresponding Author

*E-mail: e.simanek@tcu.edu.

Notes

The authors declare no competing financial interest.

ACKNOWLEDGMENTS

We thank the Robert A. Welch Foundation (A-0008) and the National Institutes of Health (R01 NIGMS 64560) for support.

REFERENCES

(1) Schellmann, N.; Deckert, P. M.; Bachran, D.; Fuchs, H.; Bachran, C. Targeted enzyme prodrug therapies. *Mini-Rev. Med. Chem.* **2010**, *10*, 887−904.

(2) Skwarczynski, M.; Hayashi, Y.; Kiso, Y. Paclitaxel prodrugs: toward smarter delivery of anticancer agents. *J. Med. Chem.* **2006**, *49*, 7253−7269.

(3) Chirgwin, J.; Chua, S. L. Management of breast cancer with nanoparticle albumin-bound (nab)-paclitaxel combination regimens: a clinical review. *Breast* **2011**, *20*, 394−406.

(4) Croom, K. F.; Dhillon, S. Bevacizumab: a review of its use in combination with paclitaxel or capecitabine as first-line therapy for HER2-negative metastatic breast cancer. *Drugs* **2011**, *71*, 2213−2229.

(5) Scripture, C. D.; Figg, W. D.; Sparreboom, A. Paclitaxel chemotherapy: from empiricism to a mechanism-based formulation strategy. *Ther. Clin. Risk Manage.* **2005**, *1*, 107−114.

(6) Baur, M.; Fazeny-Doerner, B.; Olsen, S. J.; Dittrich, C. High dose single-agent paclitaxel in a hemodialysis patient with advanced ovarian cancer: a case report with pharmacokinetic analysis and review of the literature. *Int. J. Gynecol. Cancer* **2008**, *18*, 564−570.

(7) Narita, S.; So, A.; Ettinger, S.; Hayashi, N.; Muramaki, M.; Fazli, L.; Kim, Y.; Gleave, M. E. GL12 knockdown using an antisense oligonucleotide induces apoptosis and chemosensitizes cells to paclitaxel in androgen-independent prostate cancer. *Clin. Cancer. Res.* **2008**, *14*, 5769−5777.

(8) Dhillon, T.; Stebbing, J.; Bower, M. Paclitaxel for AIDS-associated Kaposi's sarcoma. *Expert Rev, Anticancer* **2005**, *5*, 215−219.

(9) Terwogt, J. M. M.; Nuijen, B.; Huinink, W. W. T.; Beijnen, J. H. Alternative formulations of paclitaxel. *Cancer Treat. Rev.* **1997**, *23*, 87−95.

(10) Liebmann, J.; Cook, J. A.; Mitchell, J. B. Cremophor-El, Solvent for Paclitaxel, and Toxicity. *Lancet* **1993**, *342*, 1428−1428.

(11) Singla, A. K.; Garg, A.; Aggarwal, D. Paclitaxel and its formulations. *Int. J. Pharm.* **2002**, *235*, 179−192.

(12) Ganta, S.; Amiji, M. Coadministration of Paclitaxel and Curcumin in Nanoemulsion Formulations To Overcome Multidrug Resistance in Tumor Cells. *Mol. Pharmaceutics* **2009**, *6*, 928−939.

(13) Marupudi, N. I.; Han, J. E.; Li, K. W.; Renard, V. M.; Tyler, B. M.; Brem, H. Paclitaxel: a review of adverse toxicities and novel delivery strategies. *Expert. Opin. Drug Saf.* **2007**, *6*, 609−621.

(14) Guarneri, V.; Dieci, M. V.; Conte, P. Enhancing intracellular taxane delivery: current role and perspectives of nanoparticle albumin-bound paclitaxel in the treatment of advanced breast cancer. *Expert Opin. Pharmacother.* **2012**, *13*, 395−406.

(15) Dranitsaris, G.; Lidgren, M.; Lundkvist, J.; Coleman, R. Nab-paclitaxel or docetaxel; As alternatives to conventional paclitaxel for the treatment of metastatic breast cancer (MBC): A cost utility analysis in five European countries. *Value Health* **2008**, *11*, A71−A71.

(16) Edinger, D.; Wagner, E. Bioresponsive polymers for the delivery of therapeutic nucleic acids. *Wiley Interdiscip. Rev. Nanomed. Nanobiotechnol.* **2011**, *3*, 33−46.

(17) Maeda, H. Vascular permeability in cancer and infection as related to macromolecular drug delivery, with emphasis on the EPR effect for tumor-selective drug targeting. *Proc. Jpn. Acad., Ser. B* **2012**, *88*, 53−71.

(18) Gong, J.; Chen, M.; Zheng, Y.; Wang, S.; Wang, Y. Polymeric micelles drug delivery system in oncology. *J. Controlled Release* **2012**, *159*, 312−323.

(19) Zubris, K. A.; Colson, Y. L.; Grinstaff, M. W. Hydrogels as intracellular depots for drug delivery. *Mol. Pharmaceutics* **2012**, *9*, 196−200.

(20) Boas, U.; Heegaard, P. M. H. Dendrimers in drug research. *Chem. Soc. Rev.* **2004**, *33*, 43−63.

(21) Samad, A.; Alam, M. I.; Saxena, K. Dendrimers: A Class of Polymers in the Nanotechnology for the Delivery of Active Pharmaceuticals. *Curr. Pharm. Des.* **2009**, *15*, 2958−2969.

(22) Majoros, I. J.; Myc, A.; Thomas, T.; Mehta, C. B.; Baker, J. R., Jr. PAMAM dendrimer-based multifunctional conjugate for cancer therapy: synthesis, characterization, and functionality. *Biomacromolecules* **2006**, *7*, 572−579.

(23) Lim, J.; Simanek, E. E. Triazine dendrimers as drug delivery systems: From synthesis to therapy. *Adv. Drug Delivery Rev.* **2012**, *64*, 826−835.

(24) Simanek, E. E.; Abdou, H.; Lalwani, S.; Lim, J.; Mintzer, M.; Venditto, V. J.; Vittur, B. The 8 year thicket of triazine dendrimers: strategies, targets and applications. *Proc. R. Soc. London, A* **2010**, *466*, 1445−1468.

(25) Lim, J.; Lo, S. T.; Hill, S.; Pavan, G. M.; Sun, X.; Simanek, E. E. Antitumor activity and molecular dynamics simulations of paclitaxel-laden triazine dendrimers. *Mol. Pharmaceutics* **2012**, *9*, 404−412.

(26) Lim, J.; Chouai, A.; Lo, S. T.; Liu, W.; Sun, X.; Simanek, E. E. Design, synthesis, characterization, and biological evaluation of triazine dendrimers bearing paclitaxel using ester and ester/disulfide linkages. *Bioconjugate Chem.* **2009**, *20*, 2154−2161.

(27) Lim, J.; Simanek, E. E. Synthesis of water-soluble dendrimers based on melamine bearing 16 paclitaxel groups. *Org. Lett.* **2008**, *10*, 201−204.

(28) Lo, S. T.; Stern, S.; Clogston, J. D.; Zheng, J.; Adiseshaiah, P. P.; Dobrovolskaia, M.; Lim, J.; Patri, A. K.; Sun, X.; Simanek, E. E. Biological assessment of triazine dendrimer: toxicological profiles, solution behavior, biodistribution, drug release and efficacy in a PEGylated, paclitaxel construct. *Mol. Pharmaceutics* **2010**, *7*, 993−1006.

(29) van der Vlies, A. J.; Hasegawa, U.; Hubbell, J. A. Reduction-Sensitive Tioguanine Prodrug Micelles. *Mol. Pharmaceutics* **2012**, *9*, 2812−2818.

(30) Satyam, A. Design and synthesis of releasable folate-drug conjugates using a novel heterobifunctional disulfide-containing linker. *Bioorg. Med. Chem. Lett.* **2008**, *18*, 3196−3199.

(31) Vrudhula, V. M.; MacMaster, J. F.; Li, Z. G.; Kerr, D. E.; Senter, P. D. Reductively activated disulfide prodrugs of paclitaxel. *Bioorg. Med. Chem. Lett.* **2002**, *12*, 3591−3594.

(32) Lim, J.; Pavan, G. M.; Annunziata, O.; Simanek, E. E. Experimental and Computational Evidence for an Inversion in Guest Capacity in High-Generation Triazine Dendrimer Hosts. *J. Am. Chem. Soc.* **2012**, *134*, 1942−1945.

(33) (a) Pavan, G. M.; Mintzer, M. A.; Simanek, E. E.; Merkel, O. M.; Kissel, T.; Danani, A. *Biomacromolecules* **2010**, *11*, 721−730. (b) Pavan, G. M.; Barducci, A.; Albertazzi, L.; Parrinello, M. *Soft Matter* **2013**, *9*, 2593−2597.

(34) (a) Garzoni, M.; Cheval, N.; Fahmi, A. W.; Danani, A.; Pavan, G. M. *J. Am. Chem. Soc.* **2012**, *134*, 3349−3357. (b) Doni, D.; Kostiainen, M. A.; Danani, A.; Pavan, G. M. *Nano Lett.* **2011**, *11*, 723−728.

(35) Case, D. A.; Darden, T. A.; Cheatham III, T. E.; Simmerling, C. L.; Wang, J.; Duke, R. E.; Luo, R.; Walker, R. C.; Zhang, W.; Merz, K. M.; Robertson, B..; Wang, B.; Hayik, S.; Roitberg, A.; Seabra, G.; Kolossvary, I.; Wong, K. F.; Paesani, F.; Vanicek, J.; Liu, J.; Wu, X.; Brozell, S.; Steinbrecher, T.; Gohlke, H.; Cai, Q.; Ye, X.; Wang, J.; Hsieh, M.-J.; Cui, G.; Roe, D. R.; Mathews, D. H.; Seetin, M. G.; Sangui, C.; Babin, V.; Luchko, T.; Gusarov, S.; Kovalenko, A.; Kollman, P. A. *AMBER 11*; University of California: San Francisco, 2010.

(36) Jorgensen, W. L.; Chandrasekhar, J.; Madura, J. D.; Impey, R. W.; Klein, M. L. *J. Chem. Phys.* **1983**, *79*, 926−935.

(37) (a) Kasimova, A. O.; Pavan, G. M.; Danani, A.; Mondon, K.; Cristiani, A.; Scapozza, L.; Gurny, R.; Möller, M. *J. Phys. Chem. B* **2012**, *116*, 4338−4345. (b) Albertazzi, L.; Milker, F. M.; Pavan, G. M.; Salomone, F.; Bardi, G.; Panniello, M.; Amir, E.; Kang, T.; Killops, K.; Brauche, C.; Amir, R. J.; Hawker, C. J. *Biomacromolecules* **2012**, *13*, 4089−4097.

(38) Darden, T.; York, D.; Pedersen, L. *J. Chem. Phys.* **1993**, *98*, 10089−10092.

(39) (a) Ryckaert, J. P.; Ciccotti, G.; Berendsen, H. J. C. *J. Comput. Phys.* **1977**, *23*, 327−341. (b) Krautler, V.; Van Gunsteren, W. F.; Hunenberger, P. H. *J. Comput. Chem.* **2001**, *22*, 501−508.

(40) Cornell, W. D.; Cieplak, P.; Bayly, C. I.; Gould, I. R.; Merz, K. M.; Ferguson, D. M.; Spellmeyer, D. C.; Fox, T.; Caldwell, J. W.; Kollman, P. A. *J. Am. Chem. Soc.* **1995**, *117*, 5179.
(41) Mintzer, M. A.; Perez, L. M.; Simanek, E. E. Divergent synthesis of triazine dendrimers using a trimethylene-dipiperidine linker that increases efficiency, simplifies analysis, and improves product solubility. *Tetrahedron Lett.* **2010**, *51*, 1631−1634.
(42) van Dijk, M.; Rijkers, D. T.; Liskamp, R. M.; van Nostrum, C. F.; Hennink, W. E. Synthesis and applications of biomedical and pharmaceutical polymers via click chemistry methodologies. *Bioconjugate Chem.* **2009**, *20*, 2001−2016.
(43) Neef, A. B.; Schultz, C. Selective Fluorescence Labeling of Lipids in Living Cells. *Angew. Chem., Int. Ed.* **2009**, *48*, 1498−1500.
(44) Uehara, T.; Ishii, D.; Uemura, T.; Suzuki, H.; Kanei, T.; Takagi, K.; Takama, M.; Murakami, M.; Akizawa, H.; Arano, Y. gamma-Glutamyl PAMAM Dendrimer as Versatile Precursor for Dendrimer-Based Targeting Devices. *Bioconjugate Chem.* **2010**, *21*, 175−181.